Nanoscale

COMMUNICATION

View Article Online
View Journal | View Issue

Cite this: *Nanoscale*, 2015, **7**, 2271

Received 18th December 2014,
Accepted 23rd December 2014

DOI: 10.1039/c4nr07476a

www.rsc.org/nanoscale

An aerosol-based soft lithography to fabricate nanoscale silver dots and rings for spectroscopic applications†

Jeong Hoon Byeon,*[a] Dongho Park[b] and Jeong Yeol Kim[b]

Site-selective deposition of aerosol Pd nanoparticles on a substrate was employed to fabricate nanoscale Ag dots and rings through a subsequent electroless deposition. The fabricated nanoscale dot and ring arrays respectively showed properties in surface-enhanced Raman (SER, with a 1.8 × 10^5 enhancement factor) and Fourier transform near infrared (FT-NIR, at 6153 cm^{-1} absorption band) spectra.

Noble metal nanoparticles, which have unique physicochemical properties, have considerable potential for optoelectronic applications, including data storage devices, which require fine patterning of metal nanoparticles on targeted substrates.[1,2] However, the direct positioning of particles is highly intricate because, in addition to the synthesis of nanoparticles themselves, space control must also be considered.[3] Nanofabrication *via* nanopatterning on substrates both conductive and dielectric by conventional lithography,[4] has been reported in the professional literature; however, lithography is costly, intricate, and time-consuming.[5] Hence, overcoming these limitations has been sought through synthesis and subsequent patterning of a broad range of materials in pretreated substrates and templates. The generalization of these structures, however, has greatly confined the advancement of lithographic strategies.[6] Meanwhile, the process cost and environmental impact of lithographic strategies have to be resolved. One new approach that is now being considered is the design of gas-phase processes that combine fabrication nanomaterials in the gas-phase with site-selective deposition on substrates with lesser use of templates for nanodevice applications.[7–10] This approach is more attractive because there is a considerable number of temporary layers and templates in conventional lithographic processes that have to be removed to reveal the nanoscale pattern that is required.

Electroless deposition (ELD) is a representative metal deposition process for thin films and fine patterns due to its simplicity and low cost.[11] Pattern formation *via* ELD requires pretreatment with site-selective deposition to improve its applicability. The direct patterning of catalysts/seeds as initiators and ELD are complementary[12] because dielectric surfaces should be pretreated with noble metal particles prior to ELD to provide a catalyst that can reduce metal ions to atoms in an electroless bath, resulting in site-selective growth of the metal layer.[13] The representative pretreatment method for most ELD is a wet single step or two-step tin (Sn)-sensitization and palladium (Pd)-activation. However, increasing the purity of the metal layer through additional wet chemical steps and subsequent environmental impact still need to be resolved for generalization.[14,15]

In the present work, we show for the first time the possibility to synthesize silver (Ag) grains organized in nanoscale dots and rings using a technique based on aerosol lithography with Pd nanoparticles and the subsequent ELD of Ag. Unlike conventional lithographic methods that rely on many preliminary steps,[16] the present method enables fabrication of nanoscale dots and rings without much use of toxic agents and temporary layers/templates. In the case of nanodots, heating a shadow mask and cooling a target substrate can suppress mask contamination since aerosol nanoparticles tend to move to colder surfaces (selective deposition of Pd nanoparticles on a substrate, not a mask) that could make repetitive use of the mask,[17] similar to that in stencil lithography.[18] In the case of nanorings, to the best of our knowledge only a few procedures have been performed without the use of templates.[19] Briefly, aerosol Pd nanoparticles incorporating ethylene glycol (EG) droplets were first size-classified in the aerosol-state and then manipulated to produce nanoscale ring patterns of the Pd seeds on a silicon substrate for use in Ag ELD without the use of templates. Since the EG is an elastic and biocompatible material, it is suitable to be aerosolized with a spraying device, which was reported in a previous study.[20]

[a]*School of Mechanical Engineering, Yeungnam University, Gyeongsan 712-749, Republic of Korea. E-mail: postjb@yu.ac.kr; Tel: +82 53 810 2451*
[b]*Energy Conversions Technology Center, Korea Institute of Industrial Technology, Cheonan 331-822, Republic of Korea*

†Electronic supplementary information (ESI) available: The experimental procedure, SEM images of a Ag line pattern, and size distributions of EG and Pd incorporated EG nanoparticles. See DOI: 10.1039/c4nr07476a

When a plasma channel was formed between the Pd electrodes, parts of the rods evaporated and condensed into Pd primary particles. The size distributions as equivalent electrical mobility diameters of the Pd nanoparticles were measured using a scanning mobility particle sizer (SMPS, 3936, TSI, US), with the results provided in Fig. 1. The total number concentration, the geometric mean diameter, and the geometric standard deviation of the spark produced particles were 4.76×10^7 particles cm^{-3}, 12.0 nm, and 1.54, respectively. The shape and crystalline properties of the particles were analyzed using a transmission electron microscope (TEM, JEM-3010, JEOL, Japan). Prior to TEM measurements, the Pd particles were sampled on a commercial TEM grid through an electrostatic direct sampling method. The TEM measurements (Fig. 1b) verified that the morphology of the Pd particles became agglomerated structures of ultrafine single particles (~3.4 nm in lateral dimension). A representative high-magnification image (Fig. 1c) with a lattice fringe of 0.224 nm confirmed that the growth of the Pd particles occurred preferentially on the (111) plane (about 76% for 200 measured particles). Other indices also existed at Pd particles relating to their geometry under the TEM measurement, as shown in the ESI.† Another lattice fringe of Pd was 0.196 nm, which corresponds to the (200) index of the face-centered cubic Pd structure (ESI†). Voids between the ultrafine single Pd particle agglomerates may have been caused by impaction between the agglomerates and the silicon substrate. The impaction intensity of the agglomerates directed on a silicon by thermophoresis was about 10^{-19} J, which is remarkably lower than that in previous reports (more than 10^{-18} J) for splitting agglomerated aerosol structures.[21,22] This suggests that the agglomerated structures in the gas-phase consisted of weakly bonded Pd particles, which were not strong enough to maintain their agglomerated structure during thermophoretic impaction. According to a previous study,[23] agglomerate formation from spark produced particles generates weaker impaction than in other conventional cases because spark generated particles have positive charges (+0.23, the mean number of charges per particle) due to their plasma nature (*via* electron bombardment),[23] which induces weak agglomerates.

As shown in Fig. 2a, the spark-produced Pd particles were patterned on a silicon wafer through a hole of shadow mask (Fig. 2b) by thermophoretic deposition (ESI†), which is a mechanical process where particles in the gas-phase tend to move to the colder side. The Pd-patterned wafer was immersed in an ELD solution for further growth of Ag on the Pd particles. Fig. 2c displays different resolution SEM images of dot arrays of the Pd particles passed through a shadow mask. As shown in Fig. 2d, the Ag layer existed only on the Pd particles, *i.e.* the Pd-patterned area of the wafer. The Pd particles worked as catalysts to start Ag growth, and the Ag dots show that Ag grains were distributed evenly on the wafer. The Ag growth was confirmed to occur after the nucleation as the sites on the wafer were linked by deposition around these nuclei.[24] In an earlier step of the ELD, the prepatterned Pd particles worked as the anodic site where the reducing agent could be attached and oxidized. In other words, the electrons from the reducing agent that was distributed on the Pd particles and the reduced ionic Ag, resulted in Ag growth on the Pd particles. The diameters of the Ag dots (~0.27 μm) were wider than those of the Pd dots (~0.19 μm, as shown in Fig. 2c) because ELD mostly

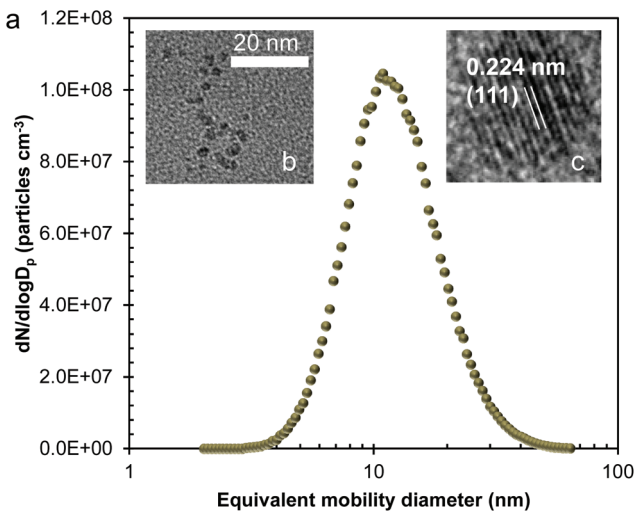

Fig. 1 (a) Particle size distribution of spark-produced Pd nanoparticles. Standard deviations are described in Table SI.† (b) Low- and (c) high-magnification TEM images of the Pd particles are shown in the insets.

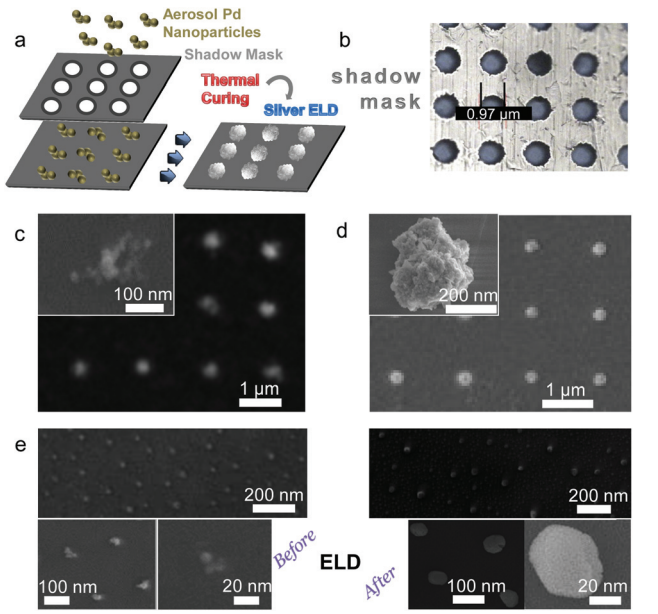

Fig. 2 Results of electroless Ag deposition on site-selectively deposited Pd particles through a shadow mask. (a) Schematics of the formation of the nanoscale Ag dots *via* the site-selective aerosol deposition of Pd nanoparticles using a shadow mask. (b) Optical microscopy image of "dot array" stainless steel shadow mask. The diameter of the hole is 0.97 μm. (c) Low- and high-magnification SEM images of the Pd "dot" patterned silicon substrate. (d) Low- and high-magnification SEM images of the Ag "dot" patterns *via* the ELD. (e) Other low- and high-magnification SEM images of the nanoscale Pd and Ag dot patterns obtained from using a different shadow mask.

works as an isotropic process (20 min of Ag ELD). This also shows that a narrower deposition (*i.e.* thermophoretic focusing) of Pd (simulation results in a previous report[17]) resulted in a dot diameter of ~0.27 μm, which is smaller than the diameter of the hole (0.97 μm) in the shadow mask. The height of the Ag dots was 146 ± 15.4 nm, which was achieved by tilting the substrate during SEM measurements. All measurements were repeated three times and reported as average values. About 46 nm in lateral dimension of Ag dots was also available by using a different shadow mask (0.1 μm hole diameter) at 10 min ELD, as shown in Fig. 2e. The morphology of Ag dots is different (Fig. 2d) from the different shadow masks because the diameter of the hole in the shadow mask did influence the size and morphology of Pd particles (left, Fig. 2e). This tendency is consistent with a previous report,[17] which introduced different electroless Ag layers from a different particle size distribution of catalyst particles.

In the case of Ag nanoring fabrication (Fig. 3a), the spark-produced Pd nanoparticles were also employed and the gas flow containing those particles was applied as the working fluid for collison atomizing diluted EG solution. The Pd particles passed through an atomizer orifice, where they merged with EG droplets to form hybrid droplets. The solvent extracted droplets were injected into an aerosol charge neutralizer (4530, HCT, Korea), and injected into a nanodifferential mobility analyzer (NDMA, 3085, TSI, US). The NDMA was employed at a fixed voltage input by an electrostatic classifier (3080, TSI, US) to sort the particles of equivalent electrical mobility. The hybrid droplets were classified at 20 nm, 80 nm (Fig. 3b), and 40 nm (Fig. 4b), and the droplets were injected into an electrostatic sampler. Fig. 3c shows TEM images (inset) of representative Pd dotted ring patterns from 80 nm size-classified droplets with different electric field intensities in the deposition chamber, and also displays SEM images of their larger areas. The migration velocity (v_{mig}) is defined by balancing the electrostatic force and the Stokes viscous force. For the size-classified Pd incorporated EG droplets, the particle migration velocity to a surface can be calculated using the following equation:

$$v_{mig} = \frac{q_p E C_c}{3\pi\mu_g D_p} \quad (1)$$

where q_p is the particle charge, E is the electric field strength, C_c is the slip correction factor, μ_g is the gas viscosity, and D_p is the particle diameter. The morphology of the Pd ring pattern varies because of the different particle velocities on the substrate, and this is consistent with our hypothesis (a higher particle velocity may cause a larger gap between the primary particles of agglomerates) regarding particle kinetic energy, already described in Fig. 1b. Unlike a previous report (employing ethanol droplets),[25] this only showed a Pd dotted structure on an EG droplet because of about a three times higher modulus elasticity of EG than that of ethanol,[26] which could hinder the penetration of Pd particles into an EG droplet during the incorporation. After thermal curing, the Pd-patterned wafer was dipped in an ELD solution, resulting in the growth of Ag on the catalysts of the wafer (Fig. 3a). Fig. 3d shows Ag nanorings after 20 min of Ag ELD from a 5 kV cm^{-1} electric field. The Ag growth occurred only on the catalysts, which is consistent with the results for Ag dot patterns. The diameter and height of the rings were 83 ± 9.3 nm and 16 ± 2.1 nm, respectively. Fig. 3e shows TEM and SEM images from size-classified Pd incorporated EG droplets at 20 nm. The Pd

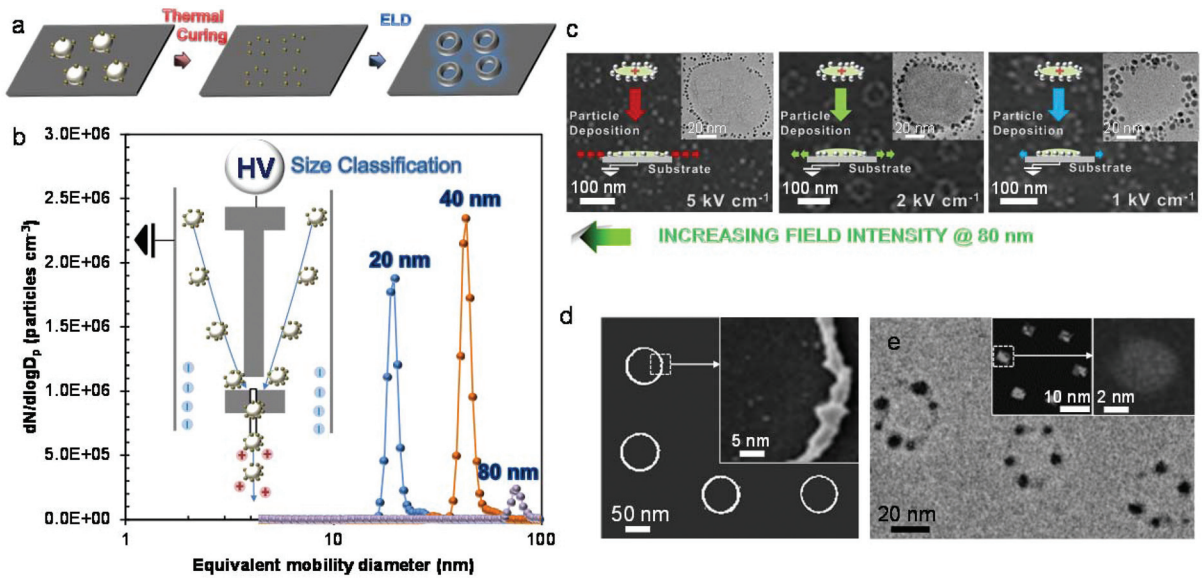

Fig. 3 Results of nanoscale Ag ring patterns *via* Pd nanoparticle hybridization with EG droplets in the aerosol-state. (a) Schematics of the formation of nanoscale Ag rings *via* aerosol hybridization. (b) Size-classification of 20, 40, and 80 nm Pd incorporated EG droplets using a NDMA. (c) SEM and TEM (inset) images of electrostatically deposited Pd incorporated EG droplets (80 nm in mobility diameter) with different electric field intensities. (d) Low- and high-magnification SEM images of the nanoscale Ag "ring" patterns from the ELD. (e) TEM image of electrostatically deposited Pd incorporated EG droplets (20 nm in mobility diameter). Insets show low- and high-magnification SEM images of the dotted Ag "ring" pattern *via* the ELD.

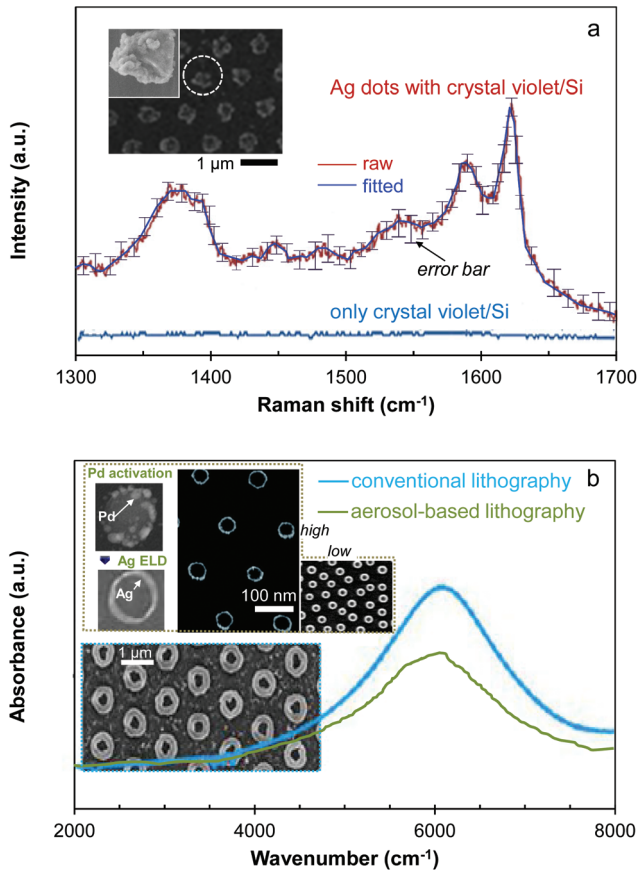

Fig. 4 SER and FT-NIR spectra of Ag patterns on the substrate. (a) SER spectrum with error bars on Ag "dot" patterns. Low- and high-magnification SEM images of the Ag "dot" patterns are also shown in the insets. (b) FT-NIR spectrum on nanoscale Ag "ring" patterns compared with a previous report (including the SEM image, bottom). Low- and high-magnification SEM images (top) of the Ag "ring" patterns are also shown in the other insets.

particles also acted as initiators for Ag ELD. Unlike size-classification at 80 nm, this showed a disconnected structure because of a lower density of Pd particles on an EG droplet. This implies that a larger hybrid droplet carried a larger number of Pd particles in the present setup; hence, the size-classification with Pd-EG incorporation should be optimized to enhance nanoring productivity. We expected that employing an aerosol conditioner, introduced in a previous report,[27] would be helpful to prepare a narrower distribution of Pd-EG hybrid droplets before size-classification. In order to enhance the regularity, the hybrid droplets may often need to be treated with unipolar gas ions or the surface needs to be modified with additional functional materials to produce wider ranges for the charges on a hybrid droplet for use in optical nanodevices, such as near infrared (NIR)-surface-enhanced Raman scattering (SERS)[28,29] and NIR-surface plasmon resonance (SPR).[30–33]

We further tested the SERS and Fourier transform (FT)-NIR properties of nanoscale Ag dots and rings because those structures are suitable for such applications. There are many approaches reported in the literature for producing SERS- and NIR-active nanoscale metallic surfaces from the fact that their SERS or SPR can be controlled by changing the size, shape, or composition of the metallic structure, effectively allowing for the control of light on the nanoscale.[34–36] In addition, an electrical resistivity of Ag line patterns was further evaluated and noted in the ESI.†

The isolated Ag nanodots (inset of Fig. 4a) have a diameter ~380 nm (30 min of Ag ELD) and consist of bunches of Ag crystals with 20–130 nm sizes and a particle density of about 5.4×10^8 cm^{-2}, measured using an siViewer (Olympus, Germany). To check the applicability of Ag nanodots as a SERS substrate, a dilute solution (10^{-3} mol L^{-1} in ethanol) of crystal violet (Sigma-Aldrich, US) was prepared and coated on the substrates. This solution was chosen as a reference material since it has an appropriate absorption band (600 nm), above the wavelength of lasers and its quantum yield of fluorescent agent is quite low, thereby appropriately excluding any fluorescent molecule background on the Raman analyses. For comparison purposes in the SERS enhancement of the nanodots (ESI†), we measured the Raman scattering of the crystal violet on a nanodot-distributed silicon surface. The measurement was performed two times at different locations, with ~16% variation between the measurements. As shown in Fig. 4a, a consistent Raman result was verified on the nanodots, showing characteristic peaks at 1370 and 1620 cm^{-1}, and the calculated SERS enhancement factor was 1.8×10^5 for the nanodots with a diameter of 380 nm and a distance of 1.3 μm between the dots, while no Raman response was shown in the absence of Ag nanodots.

Fig. 4b shows the FT-NIR absorption spectrum (Antaris II, Thermo Fisher Scientific Inc., US) from nanoscale Ag rings on a glass slide created by aerosol lithography assisted ELD. Nanorings were selected since they have unique plasmonic properties owing to strong coupling plasmons between the inner and outer surfaces.[37,38] Insets of Fig. 4b show different SEM image resolutions, which show the fabricated Ag nanorings (~55 nm diameter, ~8 nm height) on a large area. The high-magnification SEM image of a single nanoring is also shown in another inset of Fig. 4b, where the site-selective growth of Ag from the ring-shaped Pd dots (another inset of Fig. 4b, the size distribution is shown in the ESI†) is clearly seen. The nanorings are located with gaps at a distance of 40–150 nm and a ring density of ~60 μm^{-2}. The Ag rings show an absorption peak in the NIR at 6153 cm^{-1}, which were slightly different in a previous report (the bottom SEM image in Fig. 4b).[35] A difference in band position between the previous (6134 cm^{-1}) and the present results might have originated from the much smaller Ag rings than those in the previous report as well as the bimetallic (Pd–Ag core–shell) configuration in the present process.

In this work, we have presented the SER and FT-NIR spectra regarding some chosen cases, and these need to be improved further to achieve better results than those in previous reports, although the configurations of metallic nanostructures are not the same.[39] In order to improve the pattern range of the Ag nanodots and nanorings, the seed particles may often need to

be treated with ionization[40] or surface functionalization with polar components[41] to form broader ranges for the charges on a particle surface. In the case of nanorings, this strategy would be favorable to fabricate disordered arrays although the preparation steps were far fewer than conventional lithographical strategies; hence, further work regarding metal combinations (seed-overlayer, *e.g.* Ag–Au) to secure this scalability is underway based on a previous study.[42]

The fabrication of nanoscale Ag dot and ring patterns on a silicon substrate was performed *via* aerosol lithography with Pd nanoparticles and a subsequent ELD of Ag. Spark-produced Pd nanoparticles were patterned on a silicon wafer under a thermophoretic field between the particle and the wafer. The Pd-patterned wafer was then dipped in an electroless Ag solution, resulting in the growth of Ag on the previously patterned Pd (dots and rings) of the substrate. The present work offers great potential for the soft-/non-lithographic strategies of a variety of metallic nanopatterns without the need for temporary layers/templates and vacuum conditions, and thus increases the potential for future optoelectronic and sensing devices. It could be further employed in other areas, such as catalytic and antimicrobial applications.

Acknowledgements

This work was supported by the 214A054039 Yeungnam University Research Grant.

Notes and references

1 I. W. Lenggoro, H. M. Lee and K. Okuyama, *J. Colloid Interface Sci.*, 2006, **303**, 124.
2 Y.-Y. Cao, N. Takeyasu, T. Tanaka, X.-M. Duan and S. Kawata, *Small*, 2009, **5**, 1144.
3 S. Kruss, V. Srot, P. A. van Aken and J. P. Spatz, *Langmuir*, 2012, **28**, 1562.
4 J. A. Rogers and R. G. Nuzzo, *Mater. Today*, 2005, **8**, 50.
5 R. Garcia, A. W. Knoll and E. Riedo, *Nat. Nanotechnol.*, 2014, **9**, 577.
6 J.-K. Chen and J.-Q. Qui, *J. Nanopart. Res.*, 2012, **14**, 942.
7 E.-C. Lin, J. J. Cole and H. O. Jacobs, *Nano Lett.*, 2010, **10**, 4494.
8 H. Kim, J. Kim, H. Yang, J. Suh, T. Kim, B. Han, S. Kim, D. Kim, P. V. Pikhitsa and M. Choi, *Nat. Nanotechnol.*, 2006, **1**, 117.
9 S. You, K. Han, H. Kim, H. Lee, C. G. Woo, C. Jeong, W. Nam and M. Choi, *Small*, 2010, **6**, 2146–2152.
10 H. Lee, S. You, P. V. Pikhitsa, J. Kim, S. Kwon, C. G. Woo and M. Choi, *Nano Lett.*, 2011, **11**, 119.
11 J. H. Byeon, B. J. Ko and J. Hwang, *J. Phys. Chem. C*, 2008, **112**, 3627.
12 C. E. J. Cordonier, A. Nakamura, K. Shimada and A. Fujishima, *Langmuir*, 2012, **28**, 13542.
13 C. K. Srikanth and P. Jeevanandam, *Appl. Surf. Sci.*, 2009, **255**, 7153.
14 Y. Masuda, M. Kondo and K. Koumoto, *Cryst. Growth Des.*, 2009, **9**, 555.
15 J. Liu, X. Zhang, M. Yu, S. Li and J. Zhang, *Small*, 2012, **8**, 310.
16 B. Jung and W. Frey, *Nanotechnology*, 2008, **19**, 145303.
17 J. H. Byeon and J. T. Roberts, *ACS Appl. Mater. Interfaces*, 2012, **4**, 2515.
18 L. G. Villanueva, O. Vazquez-Mena, C. Martin-Olmos, V. Savu, K. Sidler, J. Montserrat, C. Hibert, P. Vettiger, J. Bausells and J. Brugger, *J. Micromech. Microeng.*, 2012, **22**, 095022.
19 N. J. Suematsu, Y. Ogawa, Y. Yamamoto and T. Yamaguchi, *J. Colloid Interface Sci.*, 2007, **310**, 648.
20 E. Ito, T. Seto, Y. Otani and H. Sakurai, *Aerosol Sci. Technol.*, 2011, **45**, 1250.
21 S. Rothenbacher, A. Messerer and G. Kasper, *Part. Fibre Toxicol.*, 2008, **5**, 9.
22 S. Froeschke, S. Kohler, A. P. Weber and G. Kasper, *J. Aerosol Sci.*, 2003, **34**, 275.
23 J. H. Byeon and J.-W. Kim, *Langmuir*, 2010, **26**, 11928.
24 S. S. Shankar, L. Rizzello, R. Cingolani, R. Rinaldi and P. P. Pompa, *ACS Nano*, 2009, **3**, 893.
25 J. H. Byeon and J. T. Roberts, *Chem. Mater.*, 2012, **24**, 3544.
26 P. N. J. Rasolofosaon and B. Zinszner, *Oil Gas Sci. Technol.*, 2012, **67**, 303.
27 J. H. Byeon, J. Hwang, J. H. Park, K. Y. Yoon, B. J. Ko, S. H. Kang and J. H. Ji, *J. Aerosol Sci.*, 2006, **37**, 1618.
28 J. Ye, M. Shioi, K. Lodewijks, L. Lagae, T. Kawamura and P. V. Dorpe, *Appl. Phys. Lett.*, 2010, **97**, 163106.
29 J. Ye, J. A. Hutchison, H. Uji-i, J. Hofkens, L. Lagae, G. Maes, G. Borghs and P. V. Dorpe, *Nanoscale*, 2012, **4**, 1606.
30 H. Jiang and J. Sabarinathan, *J. Phys. Chem. C*, 2010, **114**, 15243.
31 R. Near, C. Tabor, J. Duan, R. Pachter and M. El-sayed, *Nano Lett.*, 2012, **12**, 2158.
32 E. M. Larsson, J. Alegret, M. Käll and D. S. Sutherland, *Nano Lett.*, 2007, **7**, 1256.
33 C. Liusman, S. Li, X. Chen, W. Wei, H. Zhang and G. C. Schatz, *ACS Nano*, 2010, **4**, 7676.
34 D. Bae, W. J. Cho, G. Jeon, J. Byun and J. K. Kim, *J. Phys. Chem. C*, 2012, **116**, 26523.
35 A. R. Halpern and R. M. Corn, *ACS Nano*, 2013, **7**, 1755.
36 H.-Y. Wu, C. J. Choi and B. T. Cunningham, *Small*, 2012, **8**, 2769.
37 C. Valsecchi and A. G. Brolo, *Langmuir*, 2013, **29**, 5638.
38 M. Chirumamilla, A. Gopalakrishnan, A. Toma, R. P. Zaccaria and R. Krahne, *Nanotechnology*, 2014, **25**, 235303.
39 A. A. Semenova, E. A. Goodilin, N. A. Brazhe, V. K. Ivanov, A. E. Baranchikov, V. A. Lebedev, A. E. Goldt, O. V. Sosnovtseva, S. V. Savilov, A. V. Egorov, A. R. Brazhe, E. Y. Parshina, O. G. Luneva, G. V. Maksimovc and Y. D. Tretyakova, *J. Mater. Chem.*, 2012, **22**, 24530.
40 J. H. Byeon and J. T. Roberts, *Langmuir*, 2014, **30**, 8770.
41 S. Calder, A. Boies, P. Lei, S. Girshick and J. Roberts, *J. Chem. Mater.*, 2011, **23**, 2917.
42 J. H. Byeon and J.-W. Kim, *J. Electrochem. Soc.*, 2011, **158**, D15.